Malaysian Journal of Catalysis
http://mjcat.utm.my/
MJCat
Research Article

Photocatalytic Degradation of Phenol from Textile Wastewater Using Rutile and ZnO-NPs Doped Rutile Nanocomposite

T. L. Adewoye[1], I. A Mohammed[1], S. I. Mustapha[1] H. U. Hambali [1], A. A. Zubairu, A. S. Atanda[1], R. N. Etim [1], and B. K. Ikusemoro[1]

[1] *Department of Chemical Engineering, University of Ilorin, PMB 1515 Ilorin, Kwara Nigeria*

**Corresponding author: adewoye.tl@unilorin.edu.ng*

Article history:
Received 01 November 2024
Accepted 25 December 2024

ABSTRACT

This research focuses on the photocatalytic degradation of phenol from textile wastewater. The objective is to synthesize and characterize zinc oxide nanoparticles and rutile-ZnO-Nps nanocomposite and compare their degradation performance on phenol from textile wastewater. Zinc oxide nanoparticles (ZnO-Nps) were synthesized via a green method by mixing zinc nitrate hexahydrate with *Mangifera indica* leaf extract. The synthesized nanoparticles were incorporated into rutile (TiO_2), a photocatalyst often limited by its band gap and high recombination rate, to obtain the rutile-ZnO-Nps nanocomposite. The particle size distribution of the synthesised ZnO-Nps was assessed using dynamic light scattering (DLS) and the morphology, surface area of ZnO-Nps, pure rutile, and the rutile-ZnO-NPs nanocomposite were determined using scanning electron microscopy (SEM), and Brunauer-Emmett-Teller (BET) analysis. The photocatalytic potential of rutile and rutile-ZnO-Nps to degrade phenol from textile wastewater was investigated under three conditions: sunlight, UV lamp, and darkness. The SEM results revealed that the materials have good morphological properties and the BET results indicated that the synthesised material have relatively large surface area. The rutile-ZnO-Nps demonstrated superior photocatalytic activity under sunlight and artificial light, with degradation efficiencies of 94.87% and 91.66%, respectively, compared to pure rutile's 86.70% and 83.54%. The kinetics of phenol degradation followed pseudo-second order model suggesting chemisorption involving valence forces by sharing or exchanging electron. The doping of ZnO-Nps into rutile matrix enhanced the photocatalytic activity of the nanocomposite.

Keywords: *Photocatalyst, Pollution, Rutile nanocomposite, Textile, Wastewater*

© 2024 Faculty of Chemical and Engineering, UTM. All rights reserved
| eISSN 0128-2581 |

1. INTRODUCTION

Access to clean, safe, and sufficient freshwater is vital for the survival of all living organisms and the health of ecosystems. However, increasing global population, coupled with the expansion of industrial and agricultural activities, poses significant threats to water quality [1-2]. Freshwater accounts for only 2.5% of Earth's total water resources, and less than 1% is readily accessible for human consumption [3]. Daily activities such as urbanization, agricultural operations, and population growth generate approximately two million tons of wastewater, further straining these limited freshwater supplies [4].

Industrial advancements, particularly the discharge of untreated wastewater from major industries, exacerbate water contamination issues [5]. Among these, the textile industry is a notable contributor, generating substantial volumes of wastewater through its processes, including pre-treatment, bleaching, dyeing, and printing [6-7]. Alarmingly, over 80% of wastewater globally is discharged untreated into the environment [1]. Such indiscriminate disposal can have dire consequences for human health and aquatic ecosystems. Industrial wastewater toxins are linked to immunosuppression, reproductive disorders, acute poisoning, and waterborne diseases like cholera, typhoid, gastroenteritis, and diarrhea [8-9]. This underscores the critical need for effective wastewater treatment before discharge.

Textile wastewater is particularly challenging due to its toxicity and resistance to conventional biological treatment methods [10]. Traditional approaches, such as coagulation-flocculation [11], precipitation [12], and adsorption [13-14], are often insufficient for completely breaking down and mineralizing pollutants [15]. Consequently, photocatalytic degradation has emerged as a promising alternative. This method, which involves generating highly reactive species like hydroxyl radicals (OH•), enables the oxidation and conversion of toxic organic pollutants into less harmful substances [18]. It is considered an environmentally friendly, durable, and energy-efficient

solution, especially for treating complex, low-biodegradability wastewater with high pollutant concentrations [16-17]. Research continues to focus on developing advanced photocatalysts to enhance the efficacy of this technique.

Various metal oxide semiconductors, including TiO_2, ZnO, Fe_2O_3, CdS, ZnS, and V_2O_5, are commonly utilized in photocatalysis due to their suitable bandgap energies [19]. Among these, titanium dioxide (TiO_2) nanoparticles stand out as ideal candidates for environmental and energy-related applications. This is attributed to their distinctive properties, such as interconnected porous structures and a large surface area, which enhance their catalytic performance [20]. TiO_2 occurs in three crystalline phases: anatase, rutile, and brookite. However, brookite is rarely synthesized and seldom used as a photocatalyst due to its complex production process [21-22]. The anatase phase has been extensively studied and is preferred for photocatalytic degradation of organic pollutant due to its superior properties for oxidation reactions. In contrast, the rutile phase receives limited attention due to its comparatively lower photocatalytic efficiency.

The wide interest in TiO_2 stems from its remarkable stability, widespread availability, biological inertness, low operating temperatures, high photocatalytic activity, favorable flat-band potential, and hydrophobic nature under various environmental conditions. Additionally, its non-toxic profile makes it a sustainable choice for many applications [10]. However, a significant limitation of TiO_2 is its high electron-hole recombination rate, which reduces energy efficiency and diminishes its quantum yield [19, 23]. Several strategies have been employed to enhance the photocatalytic performance of semiconductors, including introducing dopants, sensitization, supporting them on suitable substrates, and combining different semiconductors to form composites [24]. In this study, the coupling of rutile-phase TiO_2 with ZnO nanoparticles (ZnO-Nps) was investigated to enhance the photocatalytic activity of the resulting composite. While the rutile phase has certain limitations compared to the anatase phase, it offers unique advantages, such as better sunlight absorption, lower electron mobility, and greater stability. Additionally, rutile possesses a higher density, dielectric constant, and oxygen adsorption capacity [25], making it a promising candidate for photocatalytic applications. Despite its potential, research on the photocatalytic activity of naturally occurring rutile ore remains limited.

In this work, ZnO-Nps were synthesized using a green approach that employed *Mangifera indica* leaf extract. These ZnO-Nps were then combined with rutile TiO_2 to form a rutile-ZnO-Nps nanocomposite, which was subsequently tested for the photocatalytic degradation of phenol in textile wastewater. While previous studies [26-28] have extensively focused on modifying anatase TiO_2 for the photocatalytic degradation of various pollutants, no reports, to the best of the authors' knowledge, exist on the synthesis of rutile-ZnO-Nps nanocomposites or their application for phenol degradation in real textile wastewater. This study aims to address this gap by incorporating ZnO-Nps onto rutile-phase TiO_2 to form a novel rutile-ZnO-Nps nanocomposite. The photocatalytic efficiency of pure rutile TiO_2 and the rutile-ZnO-Nps nanocomposite was compared under varying conditions to evaluate their effectiveness.

2. MATERIALS AND METHODS

2.1 Reagents

All the reagents used in this study are of analytical grade with percentage purity in the range of 97-99%, and are used without further purification. Analytical grade ethanol (C_2H_5OH), and Zinc nitrate hexahydrate ($Zn(NO_3)_2{\cdot}6H_2O$) were purchased from Sigma-Aldrich.

2.2 Collection of Sample

Mango (*Mangifera indica*) leaves served as the reducing agent in nanoparticle preparation. The leaves were obtained from disease-free mango trees in University of Ilorin campus, Kwara State. The TiO_2 (rutile) sample ore was obtained from a state in Northern Nigeria. The rutile samples were collected in representative portions, cleaned with acetone, and ground into powder using a pulverizer. The powdered samples were stored in air tight sterile sample bottles for subsequent usage.

2.2.1 *Magnifera indica* leaf extract preparation and phytochemical screening of the extract

To prepare the leaf extract, the obtained *Magnifera indica* leaves were rinsed thoroughly in running water, and then with distilled water to remove the adhered dirt. After drying at room temperature, the leaves were pulverized into fine powder using an electric blender. According to the method adopted by Elumalai & Velmurugan, [29], 20 g of powdered leaf were boiled in 100 mL distilled water for 20 min at 60°C, then cooled to room temperature. The sample was filtered using Whatman filter paper, and the filtrate was analysed for phytochemical properties using standard method described by Gupta et al. [30], and then stored in a refrigerator at 4°C until used.

2.2.2 Synthesis of Zinc oxide nanoparticles (ZnO-Nps)

The ZnO-Nps were synthesized via a green method described by Jayachandran et al [31] with slight modification. Accurately weighed, 1 g of zinc nitrate hexahydrate was added to 10 mL of the *Magnifera indica* leaf extract under steady swirling with a magnetic stirrer. After complete dissolution, the solution was heated at 65°C with a magnetic stirrer until a yellow-like colour paste was formed. The paste was then transferred to a ceramic crucible and calcined for 2 h in a furnace at 400 °C.

2.2.3 Synthesis of rutile-ZnO-Nps nanocomposite

The rutile-ZnO-Nps nanocomposite was prepared using the hydrothermal method. Firstly, 1 g of rutile was mixed with 0.5 g of ZnO-Nps in 10 mL of deionized water. The mixture was sonicated for 15 min and then separated by centrifugation for 20 min at 400 rpm. Next, the wet composite was dispersed in 20 mL of a deionized water/ethanol mixture (1:1 v/v), placed in a Teflon-lined stainless steel reactor (Autoclave), and thermally treated at 120°C for 4 h. The obtained precipitate was allowed to cool to room temperature, washed with deionized water several times, filtered and dried in an oven at 60°C for 2 h. The final product was stored in a sample bottle for subsequent use.

2.3 Characterization of the Synthesized Materials

The synthesized ZnO-Nps were characterised for their particle size distribution using Dynamic Light Scattering (DLS) Zetasizer Ver 7.01. The ZnO-Nps, pure rutile and rutile-ZnO-Nps nanocomposite were characterized for their morphology, using Scanning Electron Microscopy (SEM, Hitachi SU 3500 scanning microscope, Tokyo, Japan) using standard procedure. The particles were coated with gold under vacuum before the SEM analysis. Brunauer-Emmet-Teller (BET) Quantachrome Nova Instrument (version 11.03) was employed to determine the surface area and the pore properties using nitrogen adsorption/desorption method.

2.4 Collection and characterization of textile wastewater

Textile wastewater sample was collected from a textile industry in Lagos, Lagos state south-west, Nigeria and stored in a sealed sterile plastic container in the refrigerator at 4°C. The textile wastewater sample was characterized to determine its physicochemical properties using standard procedures. Hanna Multi-parameter instrument was employed to analyse the pH and Turbidity while the BOD level was determined using dissolved oxygen test kit.

2.5 Photocatalytic Degradation of Textile Wastewater

Degradation experiments were conducted to investigate effect of irradiation time on the degradation of phenol in textile wastewater by adding 1 g of pure rutile to series of 250 mL conical flasks, each containing 100 mL of textile wastewater sample and, the conical flasks were placed in the water-bath shaker at room temperature. The water-bath shaker was placed in a dark cupboard and the samples were shaken for 10-50 min. At a regular 10 min intervals, at the end of each reaction time, each conical flask was removed from the shaker and the textile wastewater sample was filtered to separate the used catalyst. The filtrate was then analysed for residual phenol concentration using the method described in subsequent section. The experiment was conducted under the sunlight, and UV lamp at light intensity of 20 mW/cm^3 and wavelength of 254 nm using the same procedure. This procedure was repeated with rutile-ZnO-Nps nanocomposite under the same condition and the blank experiment was also conducted under the same conditions.

The percentage removal of phenol was calculated using Equation 1

$$\%Removal = \frac{C_o - C}{C_o} \times 100 \quad (1)$$

Where C_o and C are the concentrations of the liquid before and after the degradation.

2.5.1 Total phenolic content determination

The Folin-Ciocalteu reagent was used to determine the total phenolic content in extracts. The total phenolics were quantified as mg/g gallic acid equivalents (GAE) using gallic acid as a standard. In methanol, standard solutions of known gallic acid concentrations were prepared. About 0.5 mL of the wastewater sample was measured into a clean test tube using a micro-pipette. Then, 2.5 mL of 10-fold dilute Folin-Ciocalteu reagent and 2 mL of 7.5% sodium carbonate were added to the sample in the test tube. The mixture was allowed to settle for 30 min, and the settling time had been reached, the absorbance of the mixture was obtained using the UV spectrophotometer set at a wavelength of 760 nm.

3. RESULTS AND DISCUSSION

3.1 Characterization of Textile Wastewater

Before degradation, the physico-chemical properties of the textile wastewater were evaluated to estimate the concentration of selected pollutants (COD, BOD, phenolic concentration, and heavy metals) using standard procedures described in the literature [32-34]. The results are presented in Table 1. Most parameters considered exceeded the permissible levels specified by the Federal Environmental Protection Agency (FEPA). The intense colour, and bad odour in the wastewater is detrimental to the lives of aquatic species. The high COD and BOD levels in water bodies indicate the presence of hazardous organic components. BOD is proportional to dissolved oxygen (DO), whereas COD measures the relative oxygen depletion in wastewater and this was found to be relatively high. The BOD and phenolic content are high due to oxidizable organic and inorganic compounds, and other complex mixtures of chemicals in the wastewater. Therefore, it is essential to treat the textile wastewater before being discharged to the environment to improve the quality of the wastewater and support aquatic life.

Table 1: Pollutant Concentration under different conditions

Parameters	Initial values	After treatment with Pure rutile	After treatment with rutile-ZnO-Nps	Permissible limit FEPA
Phenol (mg/L)	1.58	0.21	0.01	0.2
Odour	Offensive	Odourless	Odourless	Odourless
Colour	Dark	Clear	Clear	Clear
BOD(mg/L)	105	40	21	50.00
COD(mg/L)	210	75	56	<120
pH	8.12	6.7	7.5	6.0-9.0
Turbidity	0.5	0.42	0.34	-
Lead (mg/L)	0.8	0.4	0.2	0.05
Chromium (III)	0.56	0.43	0.32	0.05

After the treatment of the textile wastewater sample with the pure rutile and the synthesised rutile-ZnO-Nps nanocomposite adsorbent, most of the parameters

considered, except for lead and chromium fall within the permissible limit set by FEPA indicating that both rutile and rutile-ZnO-Nps nanocomposite have good potential for degrading organic pollutants in real textile wastewater while the nanocomposite displayed a better performance. Phenol was found to be considerably high (1.58 mg/L) in the textile wastewater sample, and was chosen as a representative of the pollutants for detailed photocatalytic degradation studies. Phenol is known to be a persistent organic pollutant whose presence in water is toxic to aquatic life, human life as well as other living forms [35].

3.2 Characterization of ZnO-NPs, Pure Rutile and the Composite

The ZnO-Nps was characterised for the particle size distribution using Dynamic Light Scattering (DLS). The ZnO-Nps, pure rutile and rutile-ZnO-Nps nanocomposite were analysed for surface area and morphology using Brunauer–Emmet–Teller (BET) and Scanning Electron Microscope (SEM).

3.2.1 DLS results of ZnO-Nps

The synthesized zinc oxide nanoparticle (ZnO-Nps) was characterized to determine its size distribution using DLS and the result is depicted in Figure 1. The average hydrodynamic diameter of the synthesised ZnO-Nps was found to be within nanometer range. The average particle size distribution of ZnO-Nps was 98.71 nm. Notably, the size distribution exhibited moderate dispersion, reflected by a poly-dispersity index >0.7, indicating the ZnO-Nps nanoparticle stability.

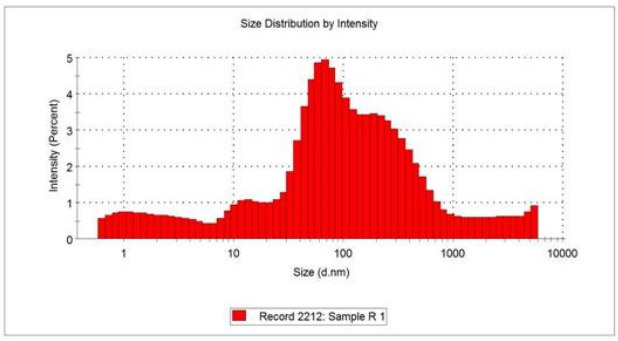

Fig. 1. DLS result for ZnO-NPs

3.2.2 BET analysis of the synthesised materials

The specific surface area, pore volume, and pore size of pure rutile, synthesised ZnO-Nps and rutile-ZnO-Nps nanocomposite were determined using Nitrogen adsorption/desorption method utilizing BET. The BET results revealed that the surface area of ZnO-Nps, rutile and rutile-ZnO-Nps is estimated to be 119.79, 921.1 and 344.52 m^2/g, respectively. The pore volume range from 0.058-0.453 cc/g and pore size was in the range of mesoporous materials (pore radius, $2 \leq r \leq 50$ nm) as specified by IUPAC. The BET results indicated that all the materials studied have good pore properties suggesting high availability of catalytic active sites for higher photocatalytic degradation activity.

3.2.3 SEM analysis of the synthesised materials

Scanning Electron Microscope (SEM) analysis was performed to determine the surface morphology of pure rutile, synthesised ZnO-Nps and rutile-ZnO-Nps nanocomposite and the SEM micrograph is presented in Figure 2. As revealed in the SEM image, the ZnO-Nps (Figure 2a) showed heterogeneous flake-like small particles forming aggregate morphology with opening. The pure rutile (Figure 2b) had a tightly packed structure with no inter-particle gap or lattice stripe. In contrast, more space voids or channels containing particles of nearly uniform sizes were observed in the rutile-ZnO-Nps nanocomposite (Figure 2c). The slight distortion of the rutile arrangement and the appearance of a loosely bound structure may be due to the coupling effect of ZnO-Nps on the rutile matrix [36]. These results suggested that the ZnO-Nps was well incorporated onto the rutile matrix which may be responsible for the better performance displayed by rutile-ZnO-Nps nanocomposite on degradation of phenol in textile wastewater.

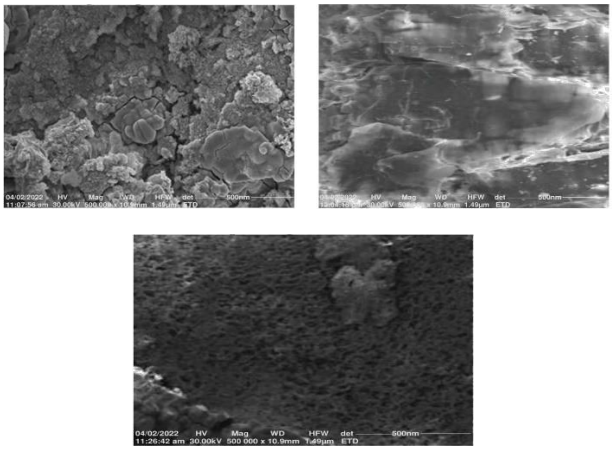

Fig. 2. SEM analysis of (a) ZnO-Nps, (b) Rutile and rutile-ZnO-Nps nanocomposite

3.3 Effect of Time on the Degradation Performance Using Pure Rutile and Rutile-ZnO-Nps nanocomposite

Photocatalytic activity was employed to evaluate the influence of time (10-50 min) on the pure rutile removal efficiency for phenol degradation. The experiment was conducted in a dark cupboard, under artificial light, and natural light irradiations by contacting 1 g of the rutile in 100 mL of textile effluent. At each time interval, samples were taken, and the residual phenol concentration was measured. Figure 3a showed that degradation efficiency increased with time under all three conditions (sunlight, UV, and dark cupboard). In the dark cupboard, removal efficiency increased with time until equilibrium was reached at 40 min,

with a maximum degradation efficiency of 79.74% on phenol degradation. Similarly, Under the UV lamps and sunlight irradiation, the efficiency increased with increase in time and attained equilibrium in 30 and 40 min, respectively with maximum degradation efficiencies of 83.54 and 86.70%, respectively on phenol degradation from textile wastewater. The relatively high degradation efficiency of pure rutile indicated the potentials of rutile TiO_2 to degrade phenol from textile wastewater. This result is comparable with the efficiency reported for phenol degradation using TiO_2 anatase phase by Eddy et al [37]; Yu& Tang [38]

Similar trend was observed with the rutile-ZnO-Nps nanocomposite for the degradation of phenol under the same condition as depicted in Figure 3b. It was noted that under the three conditions considered, the rutile-ZnO-Nps nanocomposite showed a better performance compared with the pure rutile.

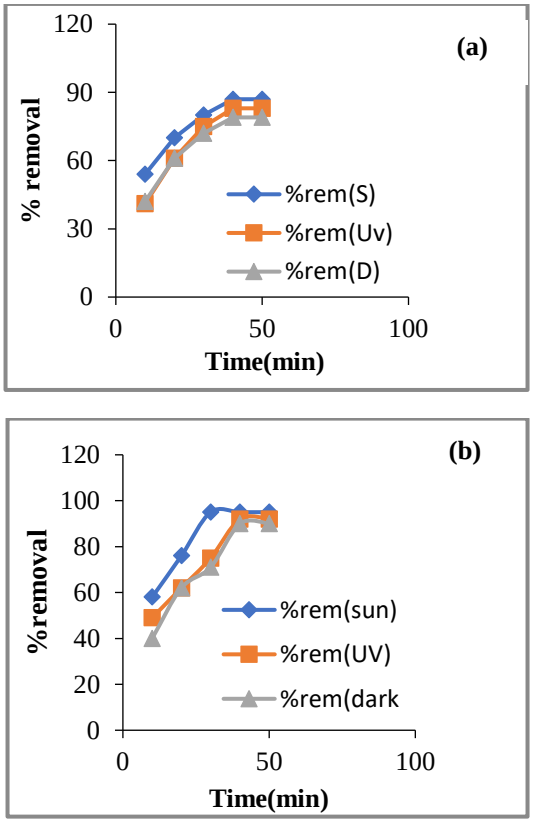

Fig. 3. Effect of time on phenol removal using (a) pure rutile and (b) Rutile-ZnO-Nps nanocomposite

In the dark cupboard, degradation efficiency of the rutile-ZnO-Nps nanocomposite also increased with time until equilibrium was attained at 40 min, achieving a maximum degradation efficiency of 89.74% on phenol. Under UV lamps and sunlight, equilibrium was attained in 30 min and the maximum degradation efficiency of rutile-ZnO-Nps nanocomposite was 91.66 and 94.87%, respectively. The degradation efficiency of the photocatalysts was significantly higher under natural sunlight than artificial light and in the dark cupboard. This may be due to higher intensity of the UV component in sunlight leading to excitation of the photocatalyst and generates more free species, enhancing degradation efficiency under sunlight compared to UV light and in dark cupboard [39]. Furthermore, rutile is known to absorb sunlight quite well, which could potentially explain why it degrades so effectively in the presence of sunlight. It was also observed that the rutile-ZnO-Nps nanocomposite reached equilibrium faster under the sunlight than the pure rutile, an evidence that the coupling of ZnO and rutile significantly enhanced the light absorption leading to an improvement in the photo-degradation efficiency of rutile-ZnO-Nps nanocomposite for degrading phenol in the textile wastewater compared to using pure rutile in agreement with Khan et al. [24] and Asefa et al. [40]. It is interesting to note that the BET surface area of the pure rutile is higher than that of rutile-ZnO-Nps nanocomposite but the results obtained in this study demonstrated that photocatalytic activity of developed catalyst is not dependent only on the surface area of the catalyst. The enhanced degradation efficiency rutile-ZnO-Nps nanocomposite may be due the decrease in electron hole recombination rate [24] as a result of the coupling of rutile with the ZnO-NPs. The combination of rutile and ZnO-Nps allows for improved electron transport from the semiconductor, which prevents recombination and increases the electrons' availability to degrade the phenol from textile wastewater [41].

3.4 Kinetic of Degradation

The kinetic of photo-degradation of phenol in textile wastewater was investigated using Pseudo-first order and pseudo-second order models according to the linear expression presented in Equation 1 and 4, respectively [19]: The kinetic of photo-degradation of phenol in textile wastewater was investigated using Pseudo-first order and pseudo-second order models according to the linear expression presented in Equation 1 and 4, respectively [19]:

$$ln\frac{C}{C_o} = -Kt \quad (2)$$

Equation 2 can be written as the expression Equation 3:

$$ln\frac{C_o}{C} = Kt \quad (3)$$

$$\frac{1}{C} - \frac{1}{C_o} = Kt \quad (4)$$

Where $\frac{1}{C} - \frac{1}{C_o}$ can be represented by $\frac{1}{C_K}$

Where C_o and C are the initial concentration of phenol in textile wastewater and final concentration after time t. K_1 and K_2 are the apparent rate constants for pseudo-first order and pseudo-second order kinetic model. The slope of Plot of $\ln {C}/{C_o}$ $vs\ t$ gives the apparent rate constant K_1 for pseudo-first order model as depicted in Figures 4 and the slope of

the plot of $\frac{1}{C_K}$ $vs\ t$ gives apparent rate constant K_2 for pseudo-second order model as presented in Figure 5.

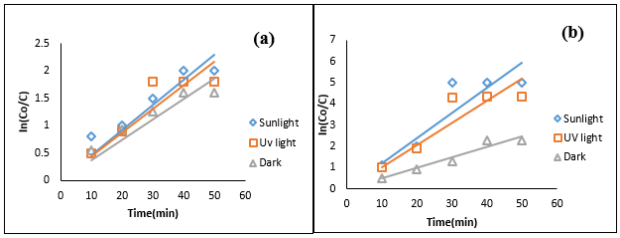

Fig. 4. Pseudo-first order plots of degradation of phenol from textile wastewater using (a) pure rutile; (b) rutile-ZnO-Nps nanocomposite.

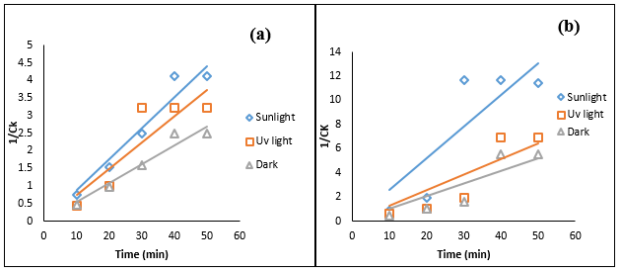

Fig. 5. Pseudo-first order plots of degradation of phenol from textile wastewater using (a) pure rutile; (b) rutile-ZnO-Nps nanocomposite.

The apparent rate constants (K_1 and K_2) and coefficients of determination (R^2) of the phenol photo-degradation under various conditions using pure rutile and rutile-ZnO-Nps nanocomposite were evaluated from Figures 4 and 5, respectively and the results are depicted in Table 2. Comparing the apparent rate constants K_1 and K_2, the K_2 obtained for pseudo-second order kinetic model were higher compared to the K_1 for pseudo-first order kinetic model using pure rutile catalyst and rutile-ZnO-Nps nanocomposite under various conditions as shown in Table 2.

Table 2: Kinetics table for the pure rutile and composite

Catalyst	Models	First Order		Second Order	
	Conditions	K_1(min^{-1})	R^2	K_2 (M^{-1}min^{-1})	R^2
Pure rutile	Sunlight	0.0460	0.7955	0.0881	0.9424
	UV light	0.0435	0.7426	0.0745	0.7895
	Dark cupboard	0.0374	0.799	0.0538	0.9479
rutile-ZnO-Nps nano-composite	Sunlight	0.1184	0.7852	0.2613	0.7367
	UV light	0.1035	0.7919	0.1291	0.7515
	Dark cupboard	0.0489	0.9351	0.1036	0.7658

Though the R^2 value obtained for pseudo-second order using rutile-ZnO-Nps nanocomposite were generally lower compared to that of pseudo-first order, the photocatalytic activity of photocatalysts can be evaluated by comparing the apparent rate constants [40]. This results suggested that the kinetic data were best fitted to the pseudo-second order model which indicated chemisorption involving valence forces by sharing or exchanging electron [42]. The apparent rate constants, K_1 and K_2 obtained for rutile-ZnO-Nps nanocomposite were higher compared to that of pure rutile which further confirmed that the rutile-ZnO-Nps nanocomposite displayed a better performance suggesting that the coupling enhanced the performance of the photocatalyst.

4. CONCLUSION

Zinc oxide nanoparticles (ZnO-NPs) were synthesized from mango leaf extract via a green synthesis route and then incorporated into rutile to produce rutile-ZnO-Nps nanocomposite. The pure rutile and the rutile-ZnO-Nps nanocomposite were characterized and used for the photocatalytic degradation of phenol from textile wastewater. The experiments were conducted under three conditions (in a dark cupboard, under UV light, and sunlight) for both photo-catalysts. ZnO-Nps were successfully synthesized from mango leaf extract and zinc nitrate hexahydrate. The nanoparticles possessed a moderately high surface area, moderate particle size distribution. ZnO-Nps were effective in the synthesis of rutile-ZnO-Nps. The characterization of the synthesized composite showed a very high surface area and pore volume, enhancing its degradation ability. Both rutile and the synthesized composite demonstrated good photocatalytic degradation ability of phenol from textile wastewater under all three conditions (dark cupboard, UV light, and sunlight). The highest removal efficiency was achieved under sunlight for both pure rutile and the rutile-ZnO-Nps nanocomposite. The results revealed that the rutile-ZnO-Nps nanocomposite performed better than pure rutile under all the conditions considered in this study. The maximum removal efficiencies of rutile-ZnO NPs for the degradation of phenol from textile wastewater were 94.87% (sunlight), 91.66% (UV light), and 89.74% (dark cupboard), while those for pure rutile were 86.70% (sunlight), 83.54% (UV light), and 79.74% (dark cupboard). The photocatalytic activity of the prepared samples, irrespective of the irradiation source, follows the order: rutile-ZnO NPs > rutile (TiO_2). The kinetic studies confirmed that the mechanism of phenol mineralization follows a pseudo-first-order kinetic model, which provided the best fit for the experimental data. The synthesised rutile-ZnO-Nps may be employed for effective photocatalytic degradation in the mineralization of textile effluent and other industrial effluents. The use of sunlight as an alternative energy source is considered as an efficient, eco-friendly, and cost effective techniques for photocatalytic degradation.

Hence, future studies could focus optimising the photocatalytic process variables.

REFERENCES

[1] N. Akhtar, M. Syakir Ishak, S. A. Bhawani, K. Umar, (2021) 19.
[2] K. D. Mello, R. H. Taniwaki, F. R. D. Paula, R. A. Valente, T. O. Randhir, D. R. Macedo, C. G. Leal, C. B. Rodrigues, R. M. Hughes, J. (2020)270.
[3] R. K. Mishra, Br. (2023) 3.
[4] J. Fito, S. W. H. Van Hulle, (2021) 3.
[5] T. Jamil, (2024) 318.
[6] N. Sharifi, M. Mohadesi, (2024) 21.
[7] H. Yin, P. Qiu, Y. Qian, Z. Kong, X. Zheng, Z. Tang, H. Guo, (2019) 7.
[8] F. O. Adeola, in: R. Haring, I. Kickbusch, D. Ganten, M. Moeti, (2021) 1–30.
[9] J. Ahmed, A. Thakur, A. Goyal, (2021) 1–14.
[10] A. A. Noaman, (2021) 4351
[11] L. Ayed, I. E. Ksibi, A. Charef, R. E. Mzoughi, (2021) 2.
[12] S. Asha, C. Hentry, M. R. Bindhu, A. M. Al-Mohaimeed, M. R. AbdelGawwad, M. S. Elshikh, (2021) 200.
[13] N. A. Bakar, N. Othman, Z. M. Yunus, W. A. H. Altowayti, M. Tahir, N. Fitriani, S. N. A. Mohd-Salleh, (2021) 22.
[14] J. Fito, S. Abrham, K. Angassa, (2020) 5.
[15] Z., Zheng, S., Tian, Y., Feng, S., Zhao, X., Li, S., Wang, Z., He, Chin. (2023) 54.
[16] A. Nyabadza, M. Makhesana, A. Plouze, A. Kumar, I. Ramirez, S. Krishnamurthy, M. Vazquez, D. Brabazon, (2024) 3.
[17] F. Tanos, A. Razzouk, G. Lesage, M. Cretin, M. Bechelany, (2024) 6.
[18] P. L. Hariani, M. Said, Salni, N. Aprianti, Y. A. L. R. Naibaho, (2022) 23.
[19] M. D. R. Vučić, J. Z.Mitrović, M. M. Kostić, N. D. Velinov, S. M. Najdanović, D. V. Bojić, A. L.Bojić , (2020) 2.
[20] V. Vasanth, K. A. Murugesh, S. Susikaran, (2022) 7. https://doi.org/10.22271/tpi.2022.v11.i7Sd.13643
[21] Z. Heydari, P. Ghadam, (2023) 43.
[22] J. Zhang, P. Zhou, J. Liu, J. Yu, (2014) 38.
[23] M. Aravind, M. Amalanathan, M. S. M. Mary, S (2021) 1 .
[24] S. Khan, A. Noor, I. Khan, M. Muhammad, M. Sadiq, N. Muhammad, (2023) 44.
[25] X. Zhang, J. Chen, S. Jiang, X. Zhang, F. Bi, Y. Yang, Y. Wang, Z. Wang, (2021) 588.
[27] H. Li, Y. Yao, X. Yang, X. Zhou, R. Lei, S. He, (2022) 45.
[28] H. M. El Sharkawy, A. M. Shawky, R. Elshypany, H. Selim, (2023) 1.
[29] K. Elumalai, S. Velmurugan, (2015) 345.
[30] M. Gupta, S. Thakur, A. Sharma, S. Gupta, (2013) 2.
[31] A. Jayachandran, T. R., Aswathy, A. S. Nair, (2021) 26.
[32] J. Ma, S. Wu, N. V. R. Shekhar, S. Biswas, A. K. Sahu, (2020).
[33] S. Mishra, A. Kumar, (2020) 1.
[34] A. Rahman, I. Jahanara, Y. N. Jolly, (2021) 2.
[35] A. I. Lawal, Z. Muhammad, C. V. Obunadike, Y. Y. Yakubu, A. O. Ogunsanmi, O. O. Abdulrazak, C. O. Ayodele, F. E. Komolafe, (2022).
[36] P. Groppe, J. Reichstein, S. Carl, C. Cuadrado Collados, B. Niebuur, K. Zhang, B. Apeleo Zubiri, J. Libuda, T. Kraus, T. Retzer, M. Thommes, E. Spiecker, S. Wintzheimer, K. Mandel, (2024).
[37] D. R. Eddy, S. N. Ishmah, M. D. Permana, M. L. Firdaus. I. Rahayu, Y. A. El-Badry, E. E. Hussein, Z. M. El-Bahy, (2021) 11.
[38] L. Yu, B. Tang, (2021) 16.
[39] J. O. Tijani, U. O. Momoh, R. B. Salau, M. T. Bankole, A. S. Abdulkareem, W. D. Roos, (2019) 19942.
[40] G. Asefa, D. Negussa, G. Lemessa, T. Alemu, J. Nanomater. T (2024).
[41] R. Beura, K. Sooraj, P. Singh, M. Ranjan, S. Mohapatra, (2024) 100595.
[42] H. D. Tran, D. G. Nguyen, P. T. Do, U. N. P. Tran, (2023) 13.